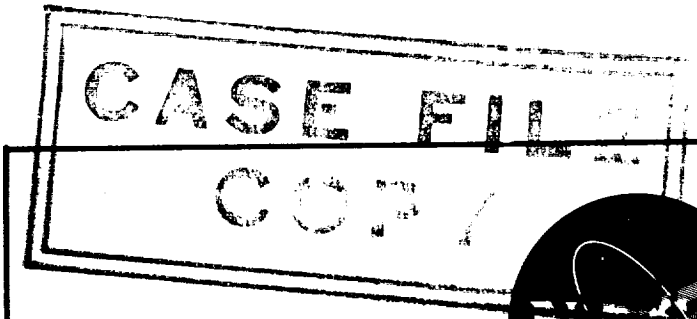

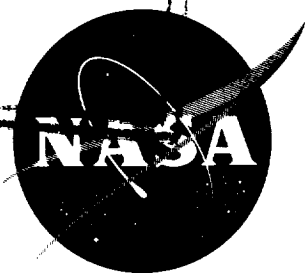

NASA TN D-1030

TECHNICAL NOTE

D-1030

AN EXPERIMENTAL TECHNIQUE FOR THE INVESTIGATION OF TIPOFF FORCES ASSOCIATED WITH STAGE SEPARATION OF MULTISTAGE ROCKET VEHICLES

By Robert L. Gungle, William S. Brosier,
and H. Wayne Leonard

Langley Research Center
Langley Air Force Base, Va.

NATIONAL AERONAUTICS AND SPACE ADMINISTRATION

WASHINGTON March 1962

NATIONAL AERONAUTICS AND SPACE ADMINISTRATION

TECHNICAL NOTE D-1030

AN EXPERIMENTAL TECHNIQUE FOR THE INVESTIGATION OF TIPOFF FORCES ASSOCIATED WITH STAGE SEPARATION OF MULTISTAGE ROCKET VEHICLES

By Robert L. Gungle, William S. Brosier,
and H. Wayne Leonard

SUMMARY

This paper presents a technique whereby tipoff disturbances which may occur during high-altitude stage separation of a multistage rocket vehicle may be readily determined from ground firings under laboratory conditions. Methods are presented for the evaluation by dynamic simulation of the combined dynamic effects of several variables arising from the proximity of the separated lower stage and the firing upper stage motor.

Expressions governing mass parameters are derived and presented in terms of relative total accelerations of the two bodies, and a discussion relating geometric parameters to the general simulation problem is given. Appropriate equations are derived which permit the conversion of observed displacements to total tipoff impulse.

Representative data presented are given in terms of the calculated total tipoff impulse necessary to produce the measured dynamic reaction of the upper stage configuration.

INTRODUCTION

The initial phase of this nation's effort to explore outer space with artificial earth satellites and probes has been hampered to a large degree by the lack of a lightweight attitude control system readily adaptable to the final or injection stage of the multistage vehicles now in use. Accordingly, the final stage has, in most cases, been provided only with spin stabilization, the effectiveness of which is a function of many parameters. Most of the multistage vehicles used to date have demonstrated a lesser degree of injection accuracy than that expected from error-analysis predictions. The continued use of multistage configurations for launching space satellites and probes necessitates the

ability to measure the disturbing forces and moments encountered at stage separation for the purpose of predicting spin-stabilized injection accuracy and, in the near future, to aid in sizing small control systems that are destined to be developed.

Experimental full-scale separation studies have been conducted during the development of many of our present-day launch configurations (ref. 1). However, due to the limitations of available test facilities, such studies have been unable to include the dynamic simulation of a thrusting rocket motor. A technique has been developed which permits the experimental investigation and evaluation of the combined dynamic effects of several basic variables on the disturbing forces and moments experienced during stage separation. These variables include nozzle misalinements, exhaust-flow conditions about the separated afterbody, mass of the upper stage, mass of the lower stage, thrust and chamber pressure of the upper stage motor, pressures of separation altitude, and in some cases the mechanics of separation.

The purpose of this paper is to discuss a test technique and the apparatus for utilizing a thrusting rocket motor in studies of tipoff forces which may occur during stage separation. Formulas are derived for simulation criteria, and a method of data reduction is presented. In addition, some representative test data are presented which were obtained during stage-separation studies of the Thor-Able, Thor-Delta, and Scout vehicles.

SYMBOLS

a acceleration, in./sec^2

A_t nozzle throat area, sq in.

C_F nozzle thrust coefficient

F force, lb

g acceleration due to gravity, in./sec^2

I mass moment of inertia about pivot point, in-lb-sec^2

k radius of gyration about pivot point, in.

l distance from pivot point to center of mass, in.

L distance from pivot point to nozzle exit plane, in.

m mass, lb-sec^2/in.

p_c rocket motor chamber pressure, lb/sq in.

H angular impulse or angular momentum, in-lb-sec

t time, sec

T thrust, lb

θ displacement angle, radians

$\overline{\theta}$ magnitude of maximum θ, radians

ψ angle between flight path and horizontal, radians

Subscripts:

a afterbody, full scale

f forebody, full scale

o initial time

r relative

s afterbody, simulated

Velocities and accelerations are denoted by single- and double-dotted quantities, respectively.

TEST TECHNIQUE AND SIMULATION CRITERIA

Basic Principles

The test technique involves the simulated firing of a representative production rocket motor at full-scale thrust and chamber pressures for a short time interval while the motor is mounted as a compound pendulum in a large vacuum vessel. Recorded time histories of the pendulous motions of the motor are then analyzed to determine the magnitude of any disturbing forces due to the motor assembly itself. In addition, the technique permits the evaluation of forces on the upper stage configuration due to the presence of an afterbody, such as the spent portion of a booster-vehicle assembly. Simulation of the afterbody is accomplished by attaching, rearward of the nozzle exit plane, a body whose mass is such that the same relative longitudinal accelerations and positions

exist between the motor and afterbody simulator as would exist between the separated stages during upper stage ignition and initial burning. Derived herein are the equations governing the mass of the afterbody simulator.

Further similitude is accomplished by constructing the afterbody simulator such that the frontal geometry of the simulator and hence the motor exhaust flow over the frontal area are equivalent to that of the flight configuration. This simulated afterbody may then be thrust away from the firing motor utilizing, where possible, the same stage separation devices as employed in the flight configuration. When the afterbody simulator has traveled sufficient distance to cease to influence the upper stage, it may then be caught by a restraining device to prevent damage to both the package and the vacuum vessel.

Simulation Criteria

Afterbody-simulator mass.- The mass of the afterbody simulator is determined in the following manner: Consider an upper stage configuration of mass m_f in proximity to an afterbody of mass m_a. Let both bodies be traveling with the same velocity along a flight path making an angle ψ with the horizontal. If the rocket motor of the upper stage is fired and T is the resultant thrust, approximately the same thrust is applied to the afterbody, but in the opposite direction, provided the frontal area of the afterbody is equal to or greater than the nozzle-exit area of the firing motor. Consider both bodies to be under the influence of a gravitational acceleration g, normal to the horizontal as shown in the following sketch:

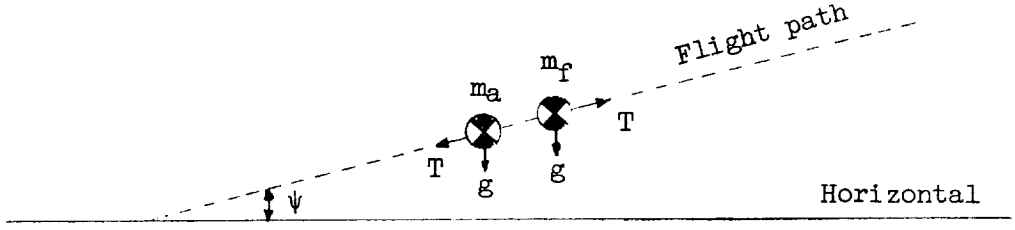

The relative acceleration of the two bodies along the flight path is the difference of the individual accelerations; or

$$a_r = a_f - a_a \tag{1}$$

where

$$a_f = \frac{T}{m_f} - g \sin \psi \tag{2}$$

and

$$a_a = -\frac{T}{m_a} - g \sin \psi \tag{3}$$

Substituting in equation (1) gives

$$a_r = \frac{\left(m_f + m_a\right)T}{m_f m_a} \tag{4}$$

Now, consider the same upper stage configuration fixed such that the thrust axis is vertical and with an afterbody simulator of mass m_s suspended directly beneath it in the same relative position as in the flight condition as shown in the following sketch:

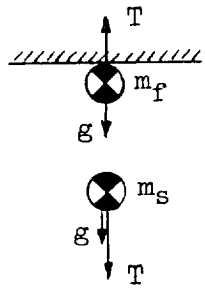

The afterbody simulator is thrust away with an acceleration

$$a_s = \frac{T}{m_s} + g \tag{5}$$

For the required simulation conditions to be satisfied, the relative longitudinal accelerations of the two bodies in each case must be equal, or

$$a_s = a_r \tag{6}$$

Substituting from equations (4) and (5) into equation (6) gives the mass of the afterbody simulator to be

$$m_s = \frac{m_f m_a T}{T(m_f + m_a) - m_f m_a g} \tag{7}$$

It is worthwhile to note that in a zero-g field, or for certain horizontal tests, the simulated afterbody mass is independent of the absolute thrust or

$$m_s = \frac{m_f m_a}{m_f + m_a} \tag{8}$$

Figure 1 illustrates the variation in mass required for a thrust range of 1,250 to 5,000 pounds (corresponding to values from 0.5T to 2T for the representative rocket motor) for two dynamic afterbodies simulated as described in a subsequent section of the present paper. The case of zero-g (eq. (8)) is also plotted for comparison with the practical case for vertical testing defined in equation (7).

Upper stage motor simulation.- Simulation of rocket motor characteristics is largely dependent upon the variables peculiar to a specific type of rocket. Close adherence to actual geometry, internal and external, as well as the inclusion of all necessary components is, of course, essential. It is then necessary to verify only the test motor chamber pressures to insure proper thrust-time simulations over the time interval of interest since the thrust is shown to be directly proportional to chamber pressure by

$$T = C_F A_t p_c \tag{9}$$

as given in reference 2, where T is the thrust, C_F is the nozzle thrust coefficient, A_t is the throat area of the nozzle, and p_c is the motor chamber pressure.

A METHOD OF DATA REDUCTION

The motor, as suspended during the tests, is equivalent to a compound pendulum subjected to an applied lateral force as shown in the following sketch:

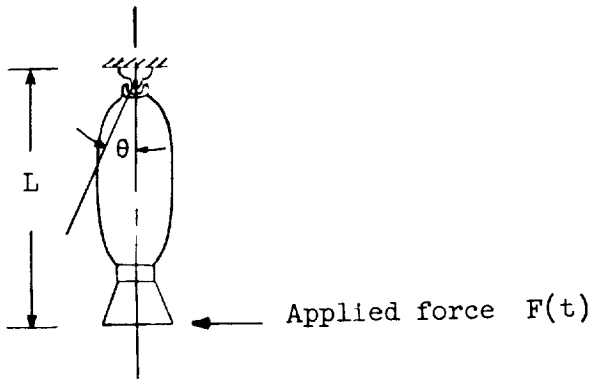

For small angular motions about the pivot point, the response of the pendulum, in a given plane, to the applied force in that plane is governed by the momentum equation for the pendulum starting from rest, which is

$$H = \int_0^t F(t)L\,dt = I\dot{\theta}(t)\Big|_{t=t} - I\dot{\theta}(t)\Big|_{t=0} \qquad (10)$$

where L is the distance from the pivot point to the nozzle exit plane, I is the mass moment of inertia about the pivot point, t is time, and θ is the displacement angle at some time t. However, since the force $F(t)$ persists for only a very short time and results in very small angular perturbations of the motor about the pivot point, the problem may be analyzed as if the pendulum were in free vibration with an initial angular velocity $\dot{\theta}_0$. The equation of motion for small-amplitude free vibration of a compound pendulum is then

$$\ddot{\theta} + g \frac{l}{k^2} \theta = 0 \tag{11}$$

having the solution

$$\theta = B \sin\left(\sqrt{\frac{gl}{k^2}}\, t\right) + D \cos\left(\sqrt{\frac{gl}{k^2}}\, t\right) \tag{12}$$

where g is acceleration due to gravity, l is the distance from the pivot point to the center of gravity, k is the radius of gyration about the pivot point, and B and D are constants determined by the initial conditions.

With the assumed initial conditions, $\theta(0) = 0$ and $\dot{\theta}(0) = H/I = H/mk^2$, equation (12) reduces to

$$\theta = \frac{H}{mk} \frac{1}{\sqrt{gl}} \sin\left(\frac{\sqrt{gl}}{k}\, t\right) \tag{13}$$

and the magnitude of maximum θ, denoted by $\bar{\theta}$, is

$$\bar{\theta} = \frac{H}{mk} \frac{1}{\sqrt{gl}} \tag{14}$$

Therefore, the total impulse of the force $F(t)$, is

$$H = mk\sqrt{gl}\ \bar{\theta} \tag{15}$$

PRACTICAL APPLICATIONS OF THE TEST TECHNIQUE

In order to illustrate the use of the technique in determining tipoff forces associated with the stage separation of rocket vehicles, tests with the Allegany Ballistic Laboratory (ABL) X248 rocket motor as the upper stage are described. The tipoff forces due to the simulated separation of this motor from three rocket vehicles - the Thor-Able, the

Thor-Delta, and the Scout vehicles - were examined. The 41-foot-diameter vacuum sphere at the Langley Research Center was used for all tests, and simulated altitudes were maintained in this vessel, which were well above those required for complete expansion of the flow in the rocket motor nozzle.

The apparatus and instrumentation for the upper stage configuration and each of the afterbody simulators are discussed separately because of the differences in the configurations dictated by the simulation criteria. All data measured in these tests were recorded on oscillograph records by cable transmission through a 3-kilocycle carrier amplifier coupled to recording elements having a flat response to 600 cps. The present state of the art yields divergent opinions as to the roll and pitch inertia simulation criteria for an assembly similar to the apparatus presented in the present paper; therefore, no attempt was made to simulate these inertias in any of the afterbody simulators.

APPARATUS AND INSTRUMENTATION

Upper Stage Configuration

The upper stage configuration consisted of an inert loaded ABL X248 rocket motor mounted as a compound pendulum. An adapter at the spindle on the nose end of the motor was connected to a needle-bearing universal joint, which was in turn connected to a thrust transducer and mounted rigidly to the top of the vacuum sphere (fig. 2). The thrust transducer was a strain-gage load cell having a 10,000-pound capacity. Variable rotary differential transformers mounted on the cross-yoke shafts of the universal joint sensed the pendulous displacements of the motor. Chamber pressures were sensed at the nose end of the motor by a differential pressure transducer, having a range of 500 lb/sq in., mounted in the resonance suppressor paddle bolt, which is vented to the propellant cavity.

The nozzle closure seal mounted in the nozzle throat was installed in the same manner as in a flight vehicle, with the exception that a nonhardening sealant was used at the nozzle lip to enable reuse of the nozzle for all tests.

The size and weight of the rocket motor simulator and the lack of readily accessible equipment prevented the measurement of geometrical nozzle alinement prior to each test. In order to circumvent this problem, the nozzle misalinement was measured several times between each series of tests as a check on assembly repeatability. The procedure for assembly of the nozzle to the rocket case was established by the motor manufacturer and strictly adhered to throughout the entire test program. The nozzle

angular misalinements measured relative to the vertical suspension axes of the test motor were random in direction and less than 0.0003 radian in magnitude. The maximum lateral displacements of the calculated centroids of the measured nozzle throat and exit planes were less than 0.006 inch. These measured angular and lateral displacements in all cases fell well within the spread measured on production rocket motors (ref. 3).

Since simulation of only the stage-separation portion of the vehicle flight was desired, only the ignition phase of motor firing was required. A method of obtaining a short burning time yielding thrust and motor chamber pressures comparable to those of the flight configuration was devised. An inert mass, which duplicates the propellant grain shape and chamber volume of a flight motor, was cast into a production X248 case by the motor manufacturer. A special igniter was then designed to produce the desired chamber pressure and thrust characteristics of the flight X248 for a minimum time of approximately 150 to 200 milliseconds of the firing sequence. The special igniter consisted of the resonance suppressor paddle on which both the stainless steel basket, containing a pyrotechnic device, and narrow strips of propellant had been mounted, as shown in figure 3. The special igniter differs from the flight igniter only in location of the basket and propellant and in the configuration of the propellant cross section.

The comparative chamber pressure data are presented in figure 4 as a function of time from initial chamber pressure rise, illustrating the high degree of chamber pressure simulation actually achieved for a minimum of 120 milliseconds. The feathered area depicts the boundary limits of chamber pressures from four simulated high-altitude qualification firings of X248 motors in the Engine Test Facility, Arnold Engineering Development Center (refs. 4 and 5), whereas the faired curves are typical chamber pressure time histories of the test motor utilizing the special igniter. The data points presented serve merely to identify the faired curves and are not indicative of the total number of data points which make up the curve. The burning time of approximately 500 milliseconds results from the complete consumption of the propellant, whereas the shorter burning time of approximately 180 milliseconds results from the consumption of a relatively small amount of the propellant.

In order to establish a more realistic basis for comparison of the several different afterbody test configurations, it was necessary to determine a reference level of disturbance inherent in the basic test assembly. This was accomplished by firing the rocket motor simulator, as shown in figure 5, with no obstructions rearward of the nozzle exit plane and measuring the resultant dynamic reaction.

Thor-Able Configuration

The Thor-Able was the first configuration tested utilizing the present technique of investigating tipoff forces produced during stage separation. Since the explosive mechanical effects of this Marman clamp separation system were under study elsewhere (ref. 6), the investigation of the National Aeronautics and Space Administration was limited to determining the contribution to total tipoff that might be expected from igniting the third-stage X248 rocket motor in close proximity to the coasting second-stage booster. The configuration consisted of a mock-up of the Thor-Able second-stage nose section suspended rigidly in a plane 8 inches rearward of the nozzle exit plane of the test rocket motor as shown in figure 6. Since the afterbody simulator was not thrust away, it was believed that the test results would be a conservative representation of the tipoff that could be expected in flight.

Instrumentation for these firings was held to a minimum and consisted primarily of the rotary transformers on the universal-joint axes. Chamber pressure was monitored only during the last two firings of this test series.

Thor-Delta Configuration

Tests to investigate the tipoff forces associated with the separation of the X248 rocket motor from the Thor-Delta vehicle provide a more sophisticated example of the use of the technique. Separation of the second and third stages of the Thor-Delta vehicle is accomplished at the end of the second-stage coast phase of the vehicle trajectory. The second and third stages are connected by petal-type doors hinged to the spin table on the second stage and connected to the third stage by a Marman clamp. At a specified time during the coast phase and after third-stage spin up, the Marman clamp is explosively removed and spin-induced centrifugal forces open the doors outward releasing the third stage. The electrical signals to the Marman clamp explosive bolts and to the third-stage igniter are simultaneous; however, because of the longer inherent delay in the rocket igniter, the petal-type doors will be partially open at the time the third-stage thrust separates the two stages. Since the effects of the explosive and mechanical action of this separation system had already been determined in the development of the vehicle (ref. 1), this portion of the separation sequence was bypassed.

The afterbody simulator for the Thor-Delta configuration was more representative of the flight system than the previously described Thor-Able simulator, in that the nose section of the simulator (fig. 7) consisted of a combination of actual flight hardware (Thor-Delta doors and spin table) and mock-ups (instrument cases, wiring, and second-stage control compartment) closely approximating the frontal geometry of the

flight system. The mass of the simulator was also made consistent with the simulation criteria as specified by equation (7).

The second-stage simulator was suspended independently of the upper stage in a position corresponding to the relative zero-acceleration coast positions of the two stages. The interstage doors were fixed in a partially opened position (see fig. 8) corresponding to the approximate position they occupy in flight at third-stage ignition. At a sensed chamber pressure, timed to insure full flow in the third-stage nozzle, the simulator was released and simultaneously thrusted upon by the motor exhaust. After traveling free about three nozzle exit diameters, the afterbody was caught by a basket-type arresting device which prevented damage to the package and vacuum vessel.

The instrumentation for these tests was more extensive than that for the Thor-Able tests. Primary instrumentation on the upper stage consisted of the rotary transformers on the universal-joint axes, motor chamber pressure and thrust transducers, and a normal-pressure transducer near the nozzle exit plane. Pressure distribution on the second-stage bulkhead, bulkhead deflections, and the longitudinal acceleration of the package were obtained from the instrumentation mounted in the mass simulator. In addition, the release of the mass simulator was monitored on the oscillograph records to insure that the proper relative position of the package was maintained until the initial exhaust pressure wave reached the nozzle exit plane.

Scout Configuration

The third example of use of the technique is the test of the Scout configuration. In this test, in addition to the effects of the physical geometry of the nose section of the lower stage and the relative motions, the mechanical separation is also simulated. The Scout fourth stage is separated in flight by using one of the many variations of a stage-separation device, generally referred to as a "blowout diaphragm." This interstage structural connection and separation device is a one-piece, externally threaded, flanged bulkhead. The bulkhead and flange are radially slotted from the major thread diameter to a stiffened center forming a number of partial circumferential segments. The stages to be joined are provided with internal threads to match the bulkhead flange and assembled so that their circumferential mating surfaces are located at the approximate midpoint of the flange thread. A circumferential overlap or shear lip is included in the stage mating parts which limits the structural load transfer from the mated stages to longitudinal and radial reactions resisted by the flange and segment stiffnesses.

Figure 9 is an example of a blowout-diaphragm installation illustrating one type of expected failure mode. Stage separation is accomplished during the initial thrust phase of the upper stage because of the pressure exerted by the rocket motor exhaust gases on the forward face of the bulkhead. The circumferential segments initially react as a series of radial beams fixed at the flange and free, but guided, at the stiffened center (fig. 9). Further deflection of the diaphragm center allows the segments to pivot about the rearward threads resulting in the release of the forward stage (fig. 9).

The simulator for the Scout third stage consisted of a package whose mass was determined by the simulation criteria of equation (7), with the interior volume mock-up as shown in figure 10. This package was mechanically attached to the upper stage by an interstage blowout diaphragm connecting the wall of the lower stage nose section to a fairing skirt attached to and extending downward from the upper stage motor case (fig. 11). The hardware of the separating mechanism (fairing skirt, blowout diaphragm, and third-stage nose chamber) closely simulated the flight articles. The separation procedure and sequence were identical to that of the flight system; that is, pressure in the interstage chamber due to initial motor burning becomes sufficient to fail the blowout diaphragm allowing the lower stage to be thrust away by the motor exhaust for approximately three nozzle exit diameters before being caught in the basket-type arresting device.

Instrumentation for the upper stage during these tests consisted of the rotary transformers on the universal-joint axes, motor chamber pressure and thrust transducers, and a normal-pressure transducer near the nozzle exit plane, as well as several pressure transducers between the nozzle and fairing skirt. In the third-stage package were three linear transformers to measure blowout diaphragm movement, three linear transformers to monitor the initial relative motion of the package to the upper stage, several transducers to monitor third-stage nose-compartment pressures, and a longitudinal accelerometer.

PRESENTATION OF REPRESENTATIVE DATA

A typical time history of the upper stage motions is presented in polar form in figure 12. This particular plot is from data obtained with the Scout third-stage simulator as the afterbody. The dashed portion of the curve represents the data obtained during motor firing whereas the solid curve represents the first cycle of the pendulous motor assembly after burnout. The numbers appearing along the solid curve indicate time in seconds from initial chamber pressure rise.

In all tests conducted there is evidence that some components of force act in both of the mutually perpendicular vertical planes whose line of intersection passes through the pivot point; however, since the perturbation angles are small, the coupling of the motion is believed to be negligible and the angle $\bar{\theta}$ is measured in that plane which contains the maximum response of the motor.

Values of the total tipoff impulse, as calculated from the experimentally determined pendulous motion by the method of equation (15), are given in figure 13 for each of the four configurations simulated. The dashed line represents the calculated level of impulse which would have resulted from the maximum measured nozzle misalinement. This maximum angular misalinement (0.0003 radian) and the lateral offset of the thrust axis would be expected to produce an impulse moment about the axes of the universal joint of 0.091 pound-second whereas the minimum observed dynamic reaction impulse moment was 0.512 pound-second. This indicates that other factors such as flow dissymmetry or gyroscopic coupling may contribute to the tipoff impulses. It is readily apparent that within the accuracy of the test data (±6 percent), no appreciable differences exist in the impulse loadings applied to the upper stage with the Thor-Able and Thor-Delta simulators as compared with those for the motor with no afterbody. The apparent increase in tipoff impulse loading for one Scout test is believed to have been contributed by the mechanical separation system employed in the Scout vehicle and simulated in these tests. It should be reemphasized that only the Scout tests in this series coupled an actual mechanical separation with the rocket motor ignition. The Thor-Able and Thor-Delta test results of this series do not reflect the possible coupling of their mechanical separation and the stage-proximity effects.

A comparison of the total impulse as determined from the simulator tests for the Thor-Delta configuration with the total impulse actually experienced by a flight vehicle was made on the basis of an error analysis performed by the Thor-Delta prime contractor on the observed orbital injection error of a Thor-Delta injected satellite. The analysis indicates that the disturbances predicted by the data presented in this report were of the correct order of magnitude to have caused the observed injection error.

Similar correlation of flight and ground test results has been obtained from an unpublished error analysis performed for a satellite orbited by the Scout vehicle.

CONCLUDING REMARKS

A technique is presented which permits the simulation and evaluation of the tipoff disturbances experienced by multistage rocket vehicles at high-altitude stage separation. Data are presented which indicate the following:

1. The tipoff disturbances occur not only in cases where the upper stage is fired in the presence of an afterbody such as a spent lower stage, but also are present when no obstructions exist rearward of the nozzle exit plane during upper stage ignition and burning.

2. Anticipated dynamic responses due solely to nozzle misalinements as measured on the test configuration do not correlate with the observed dynamic response of the system. This maximum angular misalinement (0.0003 radian) and the lateral offset of the thrust axis would be expected to produce an impulse moment about the axes of the universal joint of 0.091 pound-second whereas the minimum measured impulse moment was 0.512 pound-second. This indicates that other factors, possibly inherent in the particular rocket motor employed, and as yet unresolved, may contribute to the tipoff impulses.

Langley Research Center,
National Aeronautics and Space Administration,
Langley Air Force Base, Va., December 29, 1961.

REFERENCES

1. Moody, G. H., Porter, M. G., and Skurzynski, E. J.: Minutes for NASA Symposium on ABL X248 Motors Held at Allegany Ballistics Laboratory. Dev. 1401 (Contract NOrd 16640), Allegany Ballistics Lab., Hercules Powder Co. (Cumberland, Md.), Oct. 28-29, 1959.

2. Sutton, George P.: Rocket Propulsion Elements. Second ed., John Wiley & Sons, Inc., c.1956, p. 67.

3. Moody, G. H., Porter, M. G., and Helbert, W. B., Jr.: JATO X248 Performance Data. Dev. 1244 (Contract NOrd 16640), Allegany Ballistics Lab., Hercules Powder Co. (Cumberland, Md.), Oct. 1959.

4. Kesting, L. W.: Altitude Testing of the Allegany Ballistics Laboratory JATO X248 A2 for Project Vanguard. AEDC-TN-58-94, ASTIA Doc. No.: AD-303222 (Contract No. AF 40(600)-700), Arnold Eng. Dev. Center, Nov. 1958.

5. Morris, J. A., and Vetter, N. R.: Altitude Testing of Three ABL X248 Rockets for the NASA. AEDC-TN-59-169 (Contract No. AF 40(600)-800), Arnold Eng. Dev. Center, Jan. 1960.

6. Coombs, S. R.: Able-3 Design Test Program. TR-59-0000-00753, Space Tech. Labs., Inc., July 30, 1959.

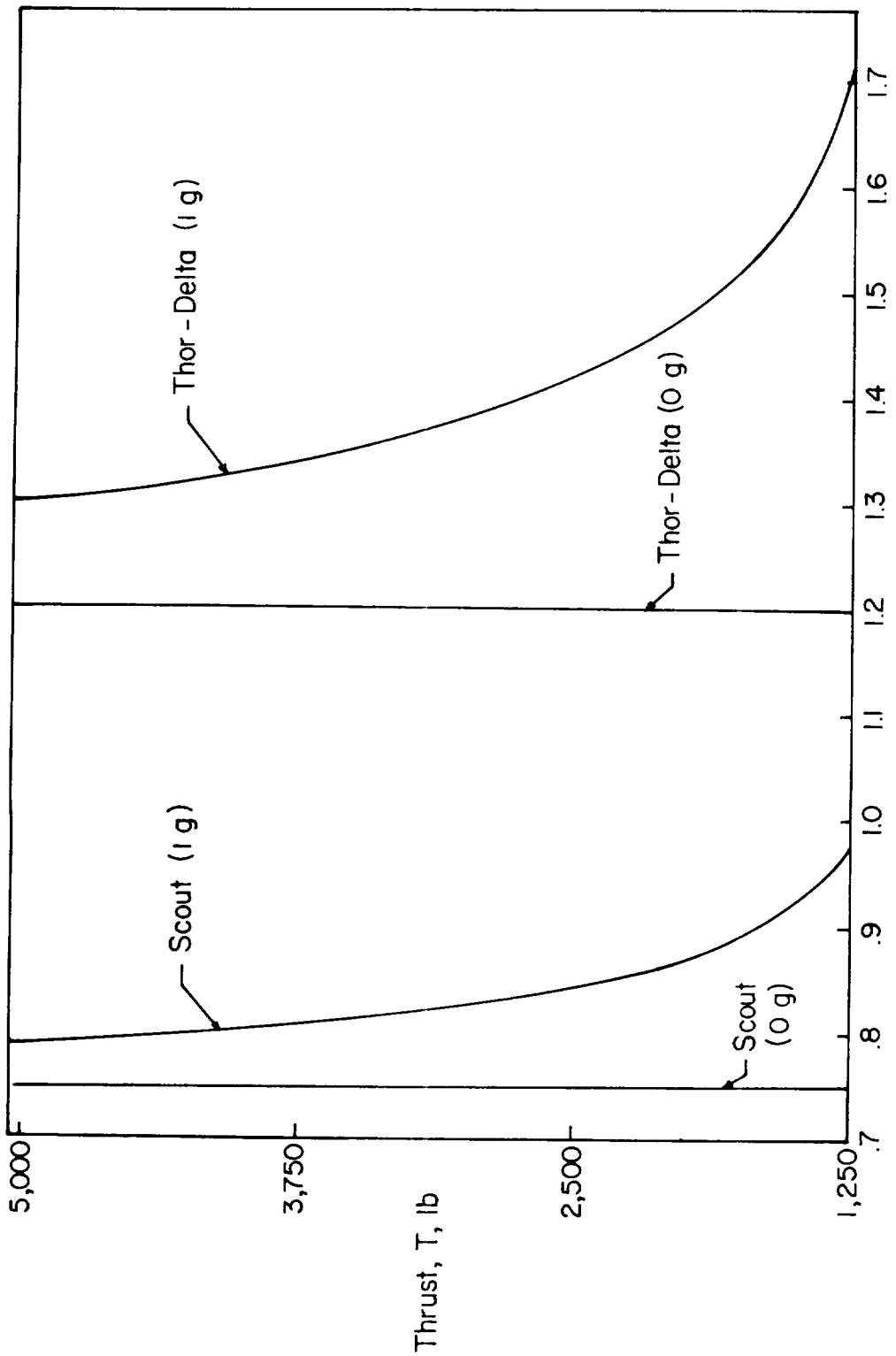

Figure 1.- Afterbody simulator mass requirements as a function of motor thrust.

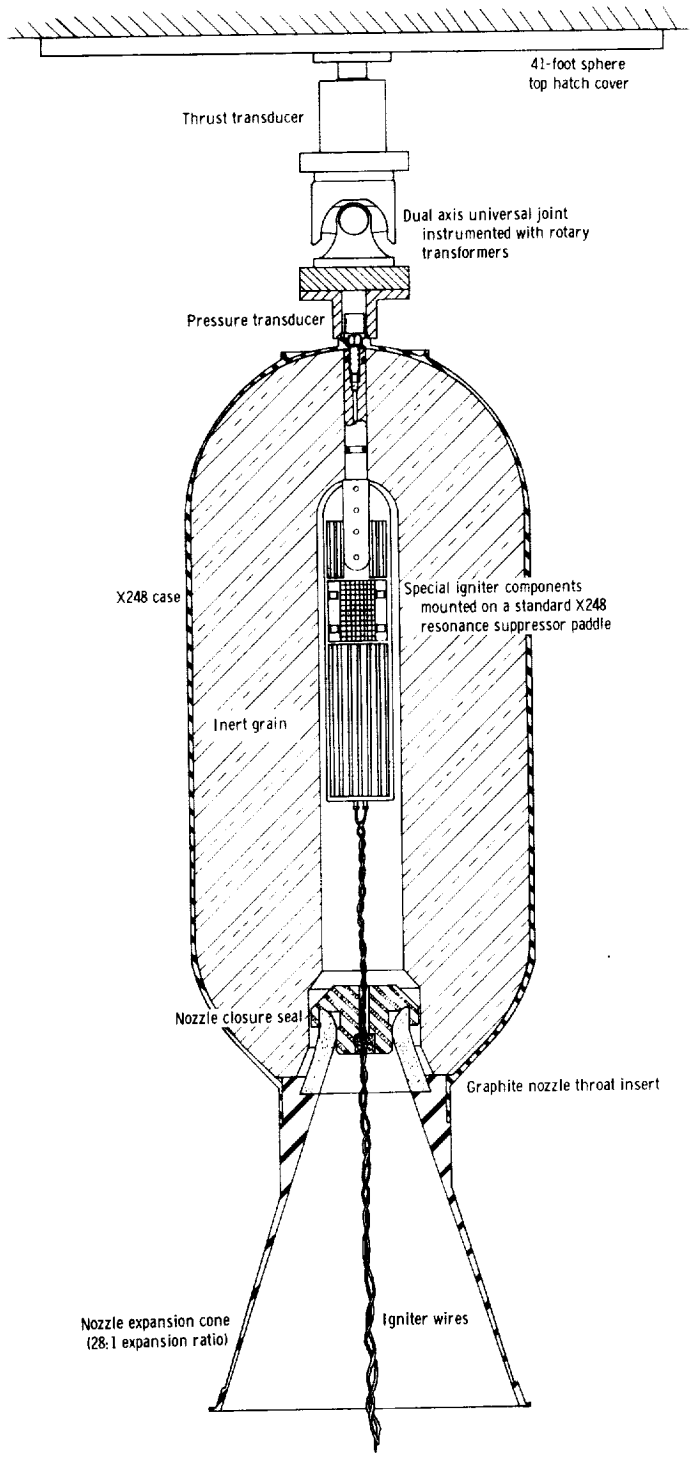

Figure 2.- Schematic illustration of basic test assembly.

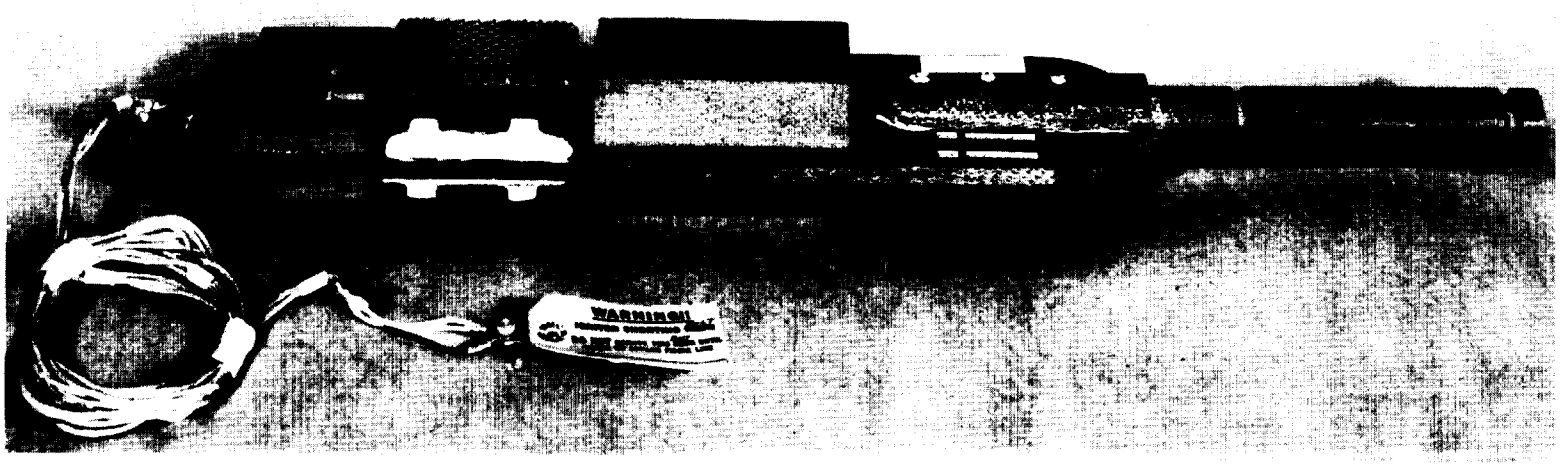

(a) Flight igniter. L-61-6007

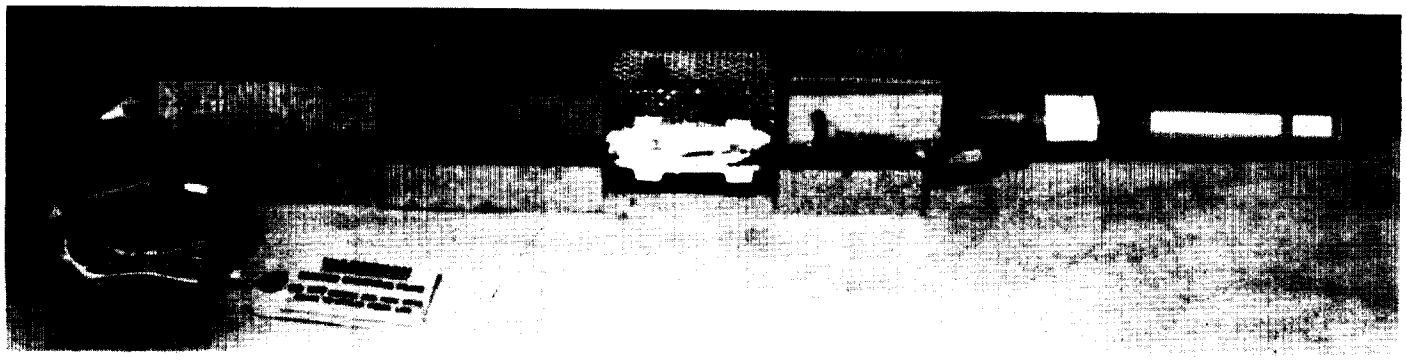

(b) Special test igniter. L-59-6532

Figure 3.- Photographs of ABL X248 igniter assemblies.

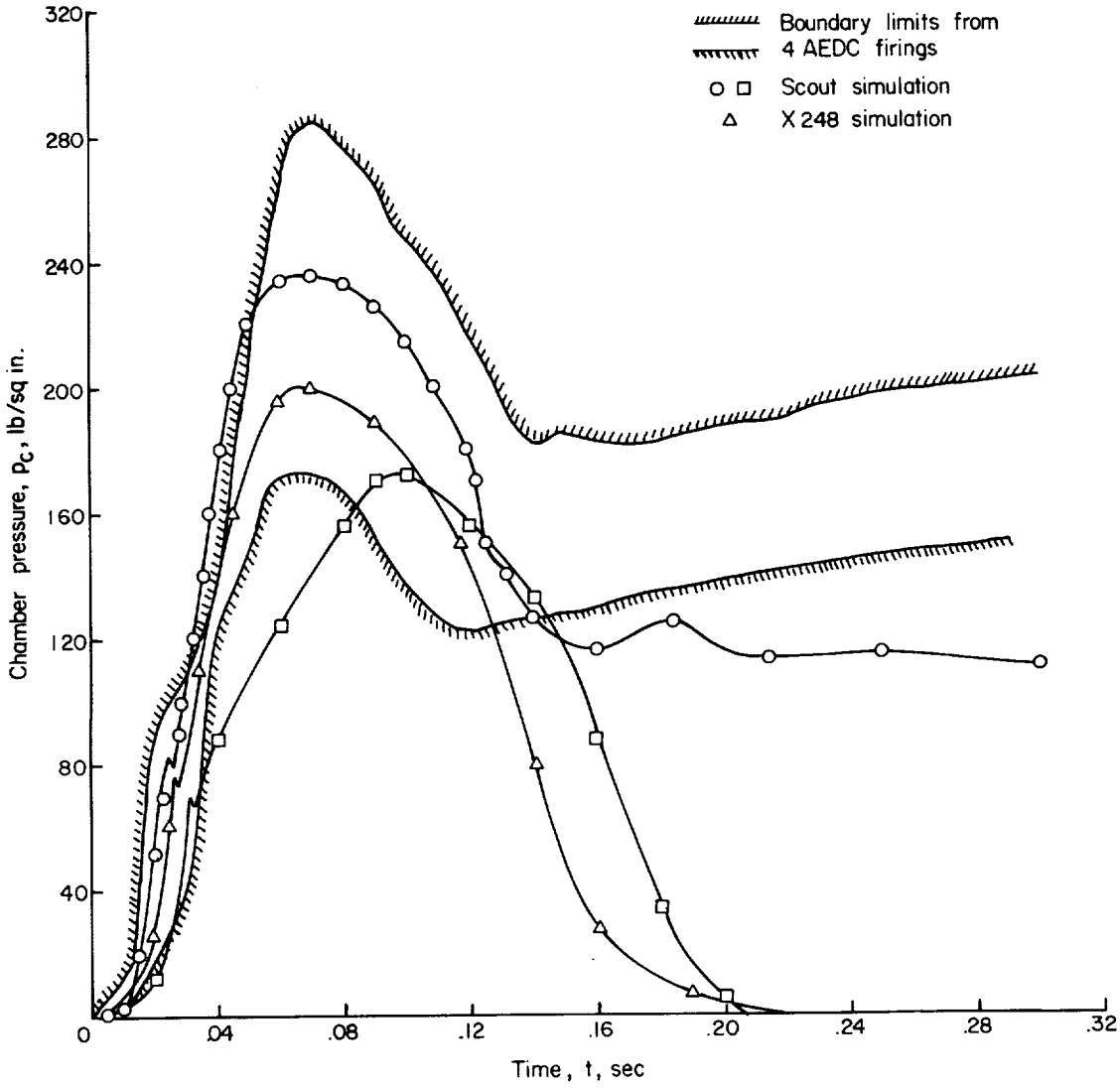

Figure 4.- Motor chamber pressure as a function of time for the test motor and for the flight ABL X248 rocket motor.

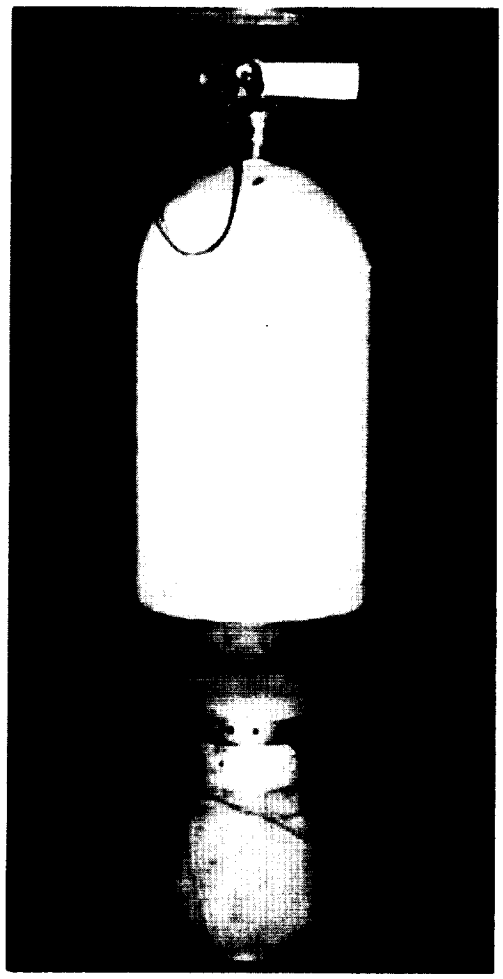

L-59-6335

Figure 5.- Basic test assembly (inert loaded ABL X248 rocket motor).

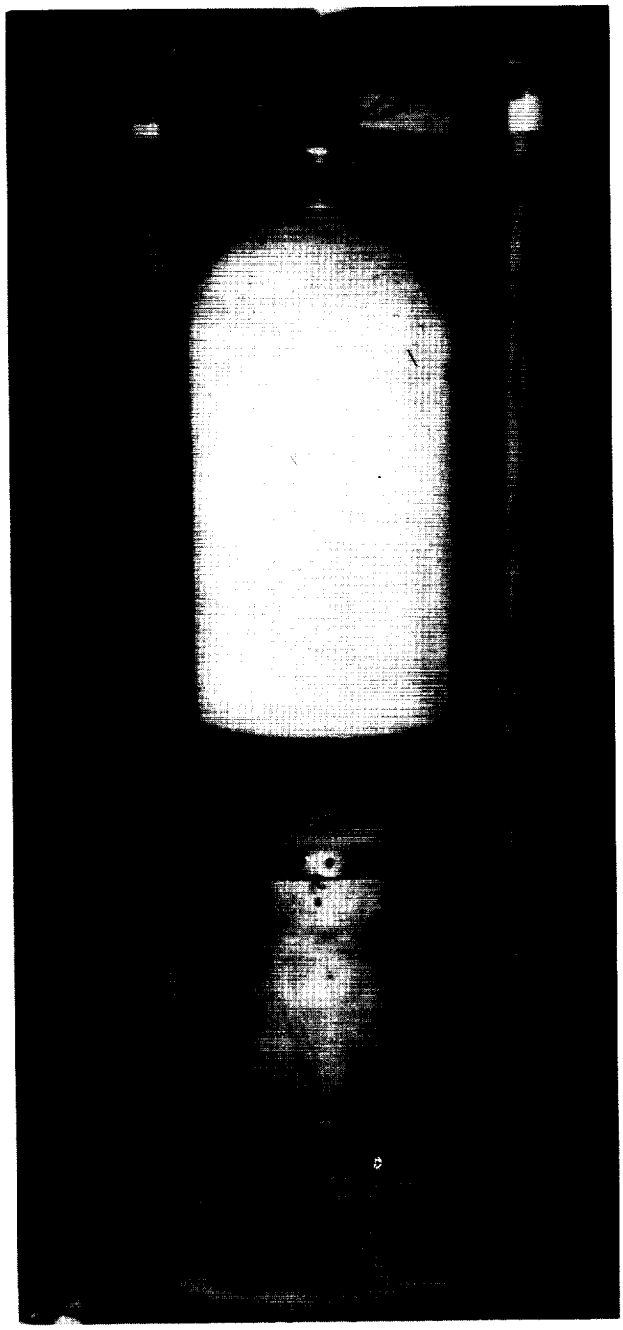

Figure 6.- Thor-Able simulation configuration. L-59-6336

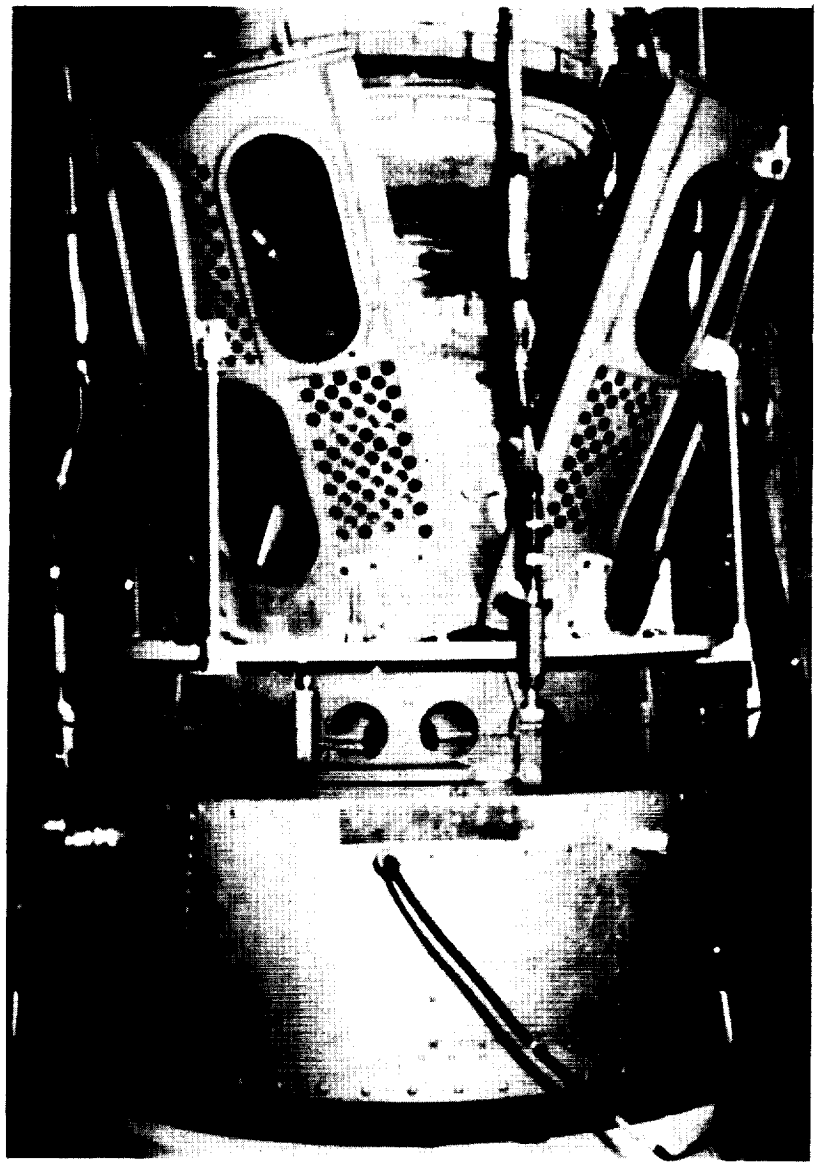

L-60-2637

Figure 7.- Thor-Delta interstage connection assembly.

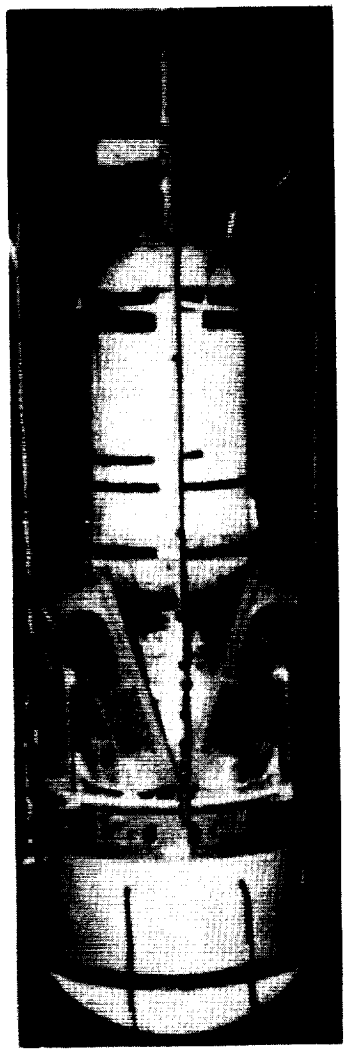

Figure 8.- Thor-Delta simulation configuration. L-60-2631

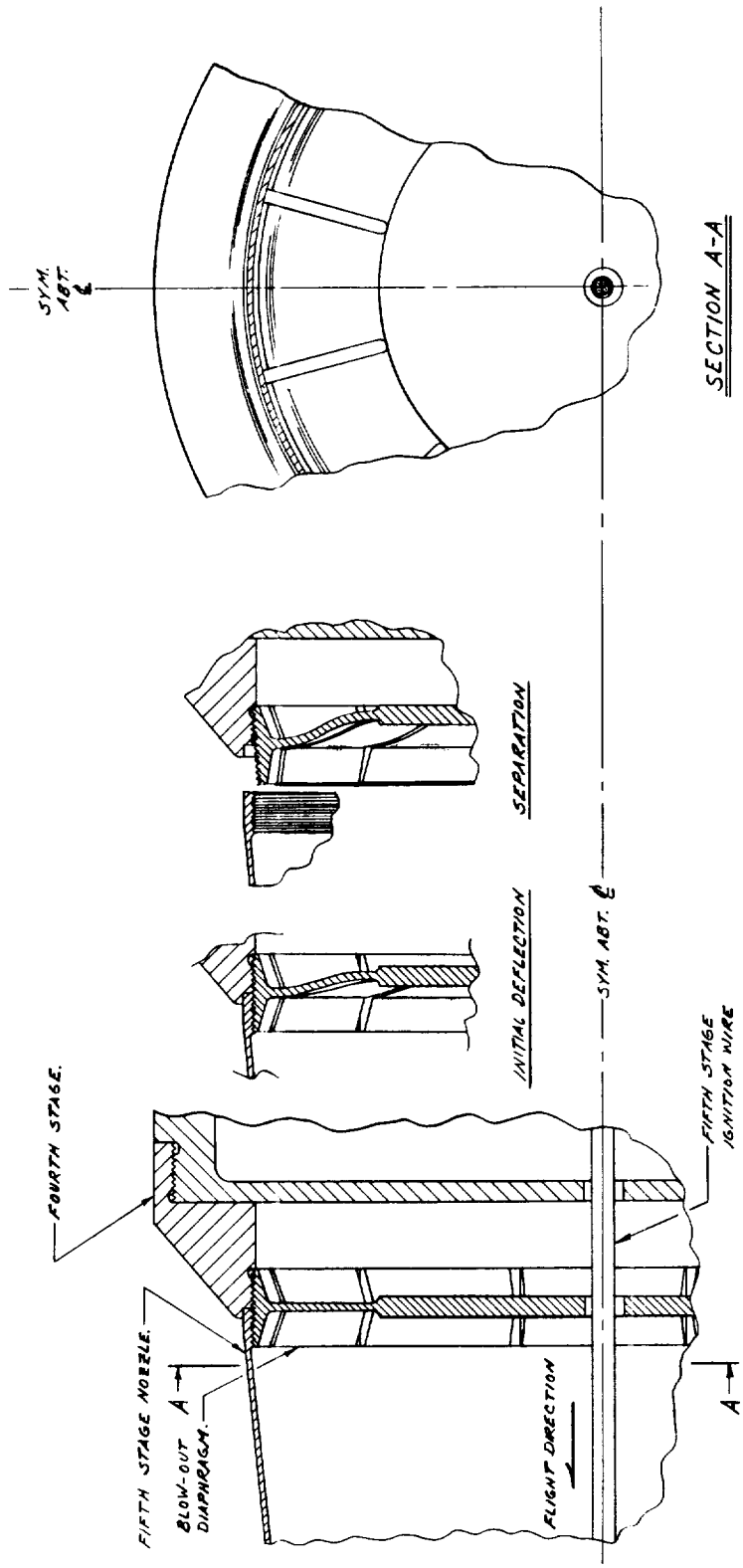

Figure 9.- Schematic illustration of general failure mode of blowout diaphragm.

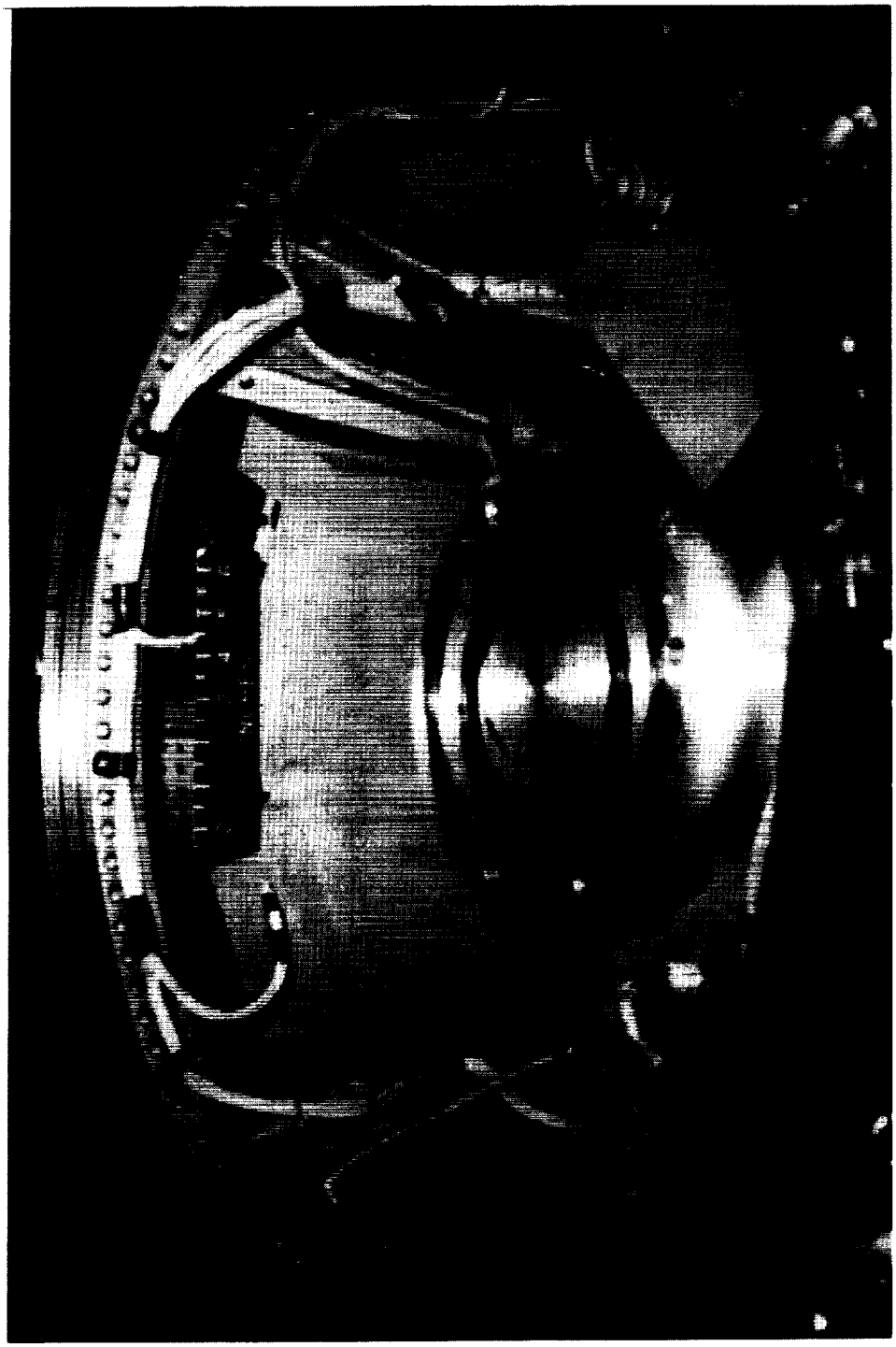

Figure 10.- Mock-up of Scout third-stage nose section. L-60-2816

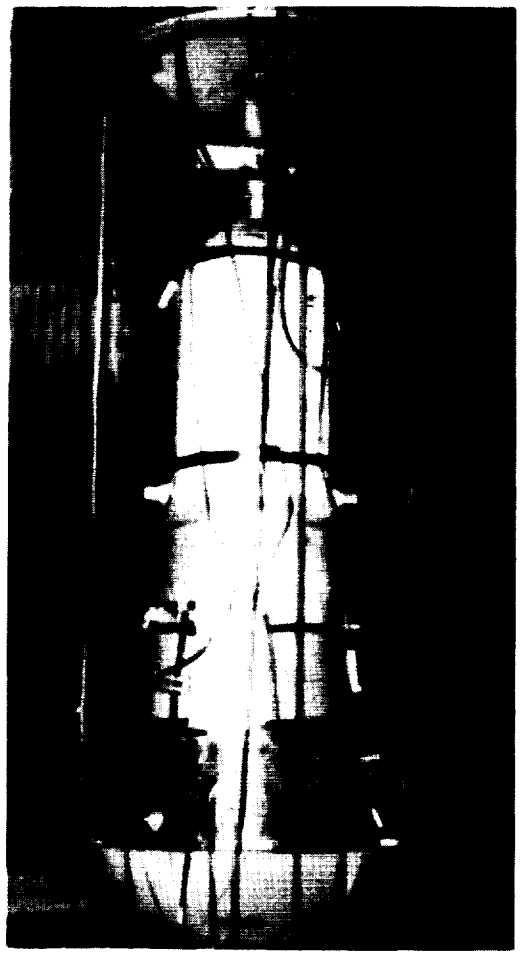

Figure 11.- Scout simulation configuration. L-60-2823

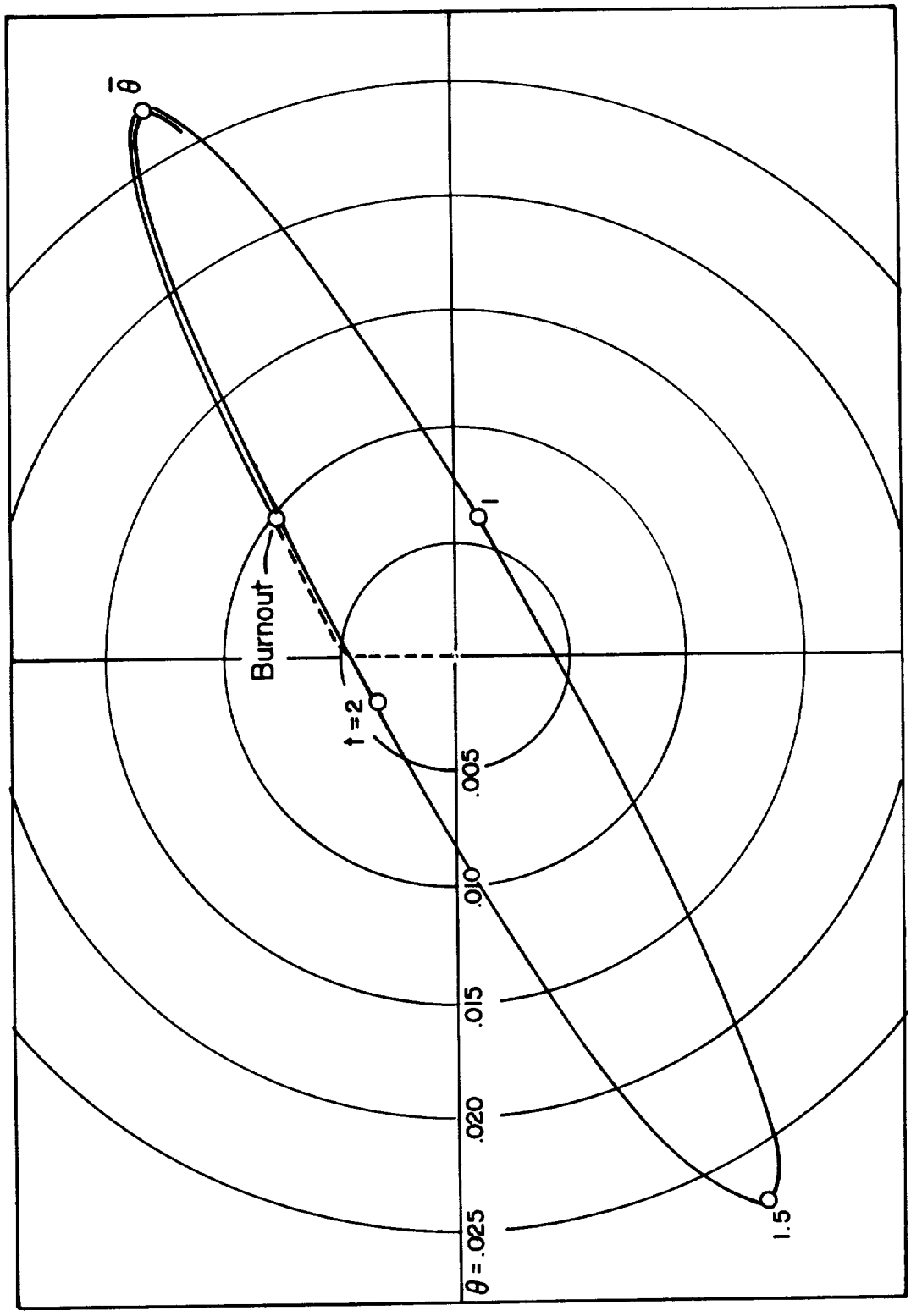

Figure 12.- Polar planform of typical motor pendulous movement.

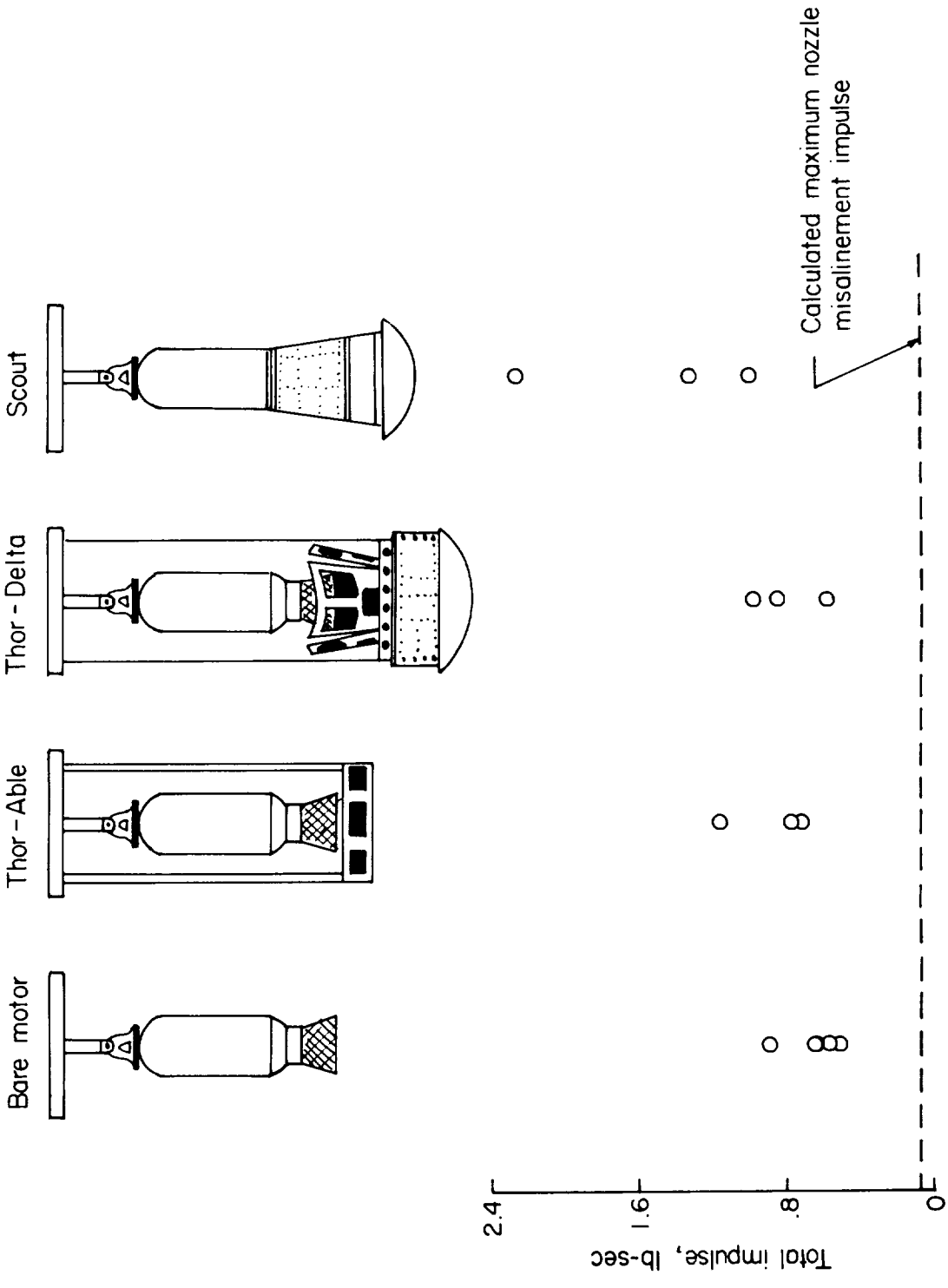

Figure 13.- Calculated total impulse for the four test configurations.

NASA-Langley, 1962 L-1667